Calculations of planar defect energies in substitutional alloys using the special-quasirandom-structure approach

Maarten de Jong, Liang Qi, David L. Olmsted, Axel van de Walle, and Mark Asta

Calculations of Planar Defect Energies in Substitutional Alloys Using the Special-Quasirandom-Structure Approach

Maarten de Jong,[1] Liang Qi,[1] David L. Olmsted,[1] Axel van de Walle,[2] and Mark Asta[1]

[1]*Department of Materials Science and Engineering, University of California, Berkeley, CA 94720*[*]
[2]*School of Engineering, Brown University, Providence, RI 02912*

A method is described for calculating the energetics of planar defects in alloys based on the special-quasirandom-structure (SQS) approach. We examine the accuracy of the approach employing atomistic calculations based on a classical embedded-atom-method (EAM) interatomic potential for hexagonal close packed (hcp) alloys, for which benchmark results can be obtained by direct configurational averaging. The results of these calculations demonstrate that the SQS-based approach can be employed to derive the concentration dependence of the energies of twin boundaries, unstable stacking faults and surfaces to within an accuracy of approximately 10 %. The SQS considered in this study contain up to 72 atoms and hence are small enough to be considered in first-principles density-functional-theory (DFT) based calculations. The application of the SQS-based approach in direct DFT-based calculations is demonstrated in a study of the concentration dependence of interfacial energies for $\{11\bar{2}1\}$ twins in hcp Ti-Al alloys.

I. INTRODUCTION

Dislocation slip and deformation twinning are the most commonly observed mechanisms for plastic deformation in metals and alloys. Which of these mechanisms dominates for a given material and loading condition is generally governed by the ease of nucleation of the relevant defects, and their growth and propagation. These processes are in turn strongly influenced by the energetics of planar defects, such as generalized stacking faults and twin boundaries. The competition between plastic deformation and fracture, underlying the intrinsic ductility of a material, is thus commonly investigated through the consideration of the relative values of the energies for relevant planar faults and the free surfaces formed by crack propagation[1–4].

For example, in the theory of Thomson and Rice[2,5], larger values of the ratio of the surface energy (γ_s) to the unstable stacking fault energy (γ_USF) are an indicator of increasingly ductile behavior, as γ_USF corresponds to the barrier for dislocation slip at the crack tip, while γ_s measures the increase in surface energy due to crack growth. This theory has been used in the literature to study the ductility in metals from first principles (e.g.[6,7]). Similarly, for hcp metals larger values of the ratio γ_s/γ_t between surface and twin-boundary (γ_t) energies have been shown to correlate with higher ductility under conditions where twinning at the crack tip is the relevant mechanism for plastic deformation[8]. For body centered cubic (bcc) and face centered cubic (fcc) materials, similar measures of twinnability have been developed and employed, which are based on (unstable) stacking fault energies and unstable twin energies[7,9–12].

In applications of computational modeling to guide alloy design, methods for calculating the effect of composition on the planar fault energies defined above are useful to understand whether the introduction of specific solute species will tend to increase or decrease the ductility and strength of a given material. However, the calculation of planar defect energies in alloys is considerably more difficult than for elemental metals or ordered intermetallic compounds, due to the presence of configurational substitutional disorder, leading to a lack of translational periodicity. At present, two main approaches have been introduced for computing the composition dependence of planar defect energies in alloy solid solutions from first-principles.

In the first, stacking fault energies in alloys have been computed within the axial next-nearest-neighbor Ising (ANNNI) lattice-model formalism[13–26]. In this approach, the energies of fcc, hcp and double-hcp structures are computed to derive pairwise interactions that parametrize the change in energy associated with different stacking sequences of close-packed planes. Once derived from bulk energy calculations, these interactions are used to predict the excess energy of an isolated stacking fault. This method has been used for alloys, in which case the special-quasirandom-structure (SQS) approach[27–29] has been used to model the energetics of compositionally disordered fcc, hcp and double hcp structures[27–31]. While this approach provides a powerful framework for computing the composition dependence of stable stacking fault energies, it is not possible to apply the method to calculations of unstable stacking fault energies, defined as the energy maximum in the generalized-stacking-fault (GSF) surface. Further, it is not apparent how to generalize the approach in the consideration of the energies of surfaces, or the large variety of twin boundaries observed in the deformation of hcp metals.

Another approach that has been employed to compute planar defect energies in alloys is based on the use of the coherent potential approximation (CPA)[32–34]. In applications of the CPA to the calculation of energies of bulk alloys, a disordered substitutional arrangement of atoms over the sites of a parent lattice is modeled using a single effective atomic species defined to have the average electron-scattering properties of the alloy. This procedure restores the translational symmetry of the under-

lying parent lattice, facilitating direct DFT calculations of bulk alloy energetics. The CPA approach has been generalized to consider layered structures, to enable calculations of stacking fault (stable and generalized) and surface energies[32,35–43]. At present, however, the implementations of the approach do not allow for the accurate treatment of atomic displacements and the generalization of the method to general low-symmetry twin boundaries, such as those found in hcp metals, for which significant atomic shuffles may arise, has not been demonstrated to the best of our knowledge.

In the present work we describe an approach for calculating the energies of planar defects in disordered substitutional alloys, based on a generalization of the SQS method[27,28] developed to compute the electronic structure and energetics of bulk substitutional alloys. Compared to previously employed methods, the present approach offers the advantage that it readily enables consideration of arbitrary crystal structures; for example, most of the previous work on this topic has considered fcc materials, while in the present work we demonstrate applications to lower-symmetry hcp structures. It should be noted that the intended application of the approach outlined in this work is to compute planar fault energies in solid solutions relevant to deformation processes at low temperatures. Hence, we do not consider the effect of configurational rearrangements and segregation on planar-fault energetics. In other words, the approach is intended to be applied to situations where planar faults form, e.g., due to glide of dislocations, on time scales for which the the atomic configuration can be considered "frozen in" due to the slow rate of atomic interdiffusion. Also, we note that the SQS-based approach presented here is demonstrated for non-spin-polarized binary solid solutions; extensions of the approach to the consideration of multicomponent alloys and/or spin degrees of freedom are beyond the scope of the present work.

The approach presented in this work was demonstrated recently in applications to the calculation of twin-boundary and surface energies in hcp Re-based alloys[44]. In this paper we describe a refinement of the approach, employing planar averaging, and provide details of the SQS structures used in the method. Further, we demonstrate the application of this approach also in the study of unstable stacking fault and surface energies. We present a test of the accuracy of the approach, through comparisons with large-supercell benchmark results derived employing a classical embedded-atom-method (EAM) interatomic potential model for Ti-Al alloys[45]. Finally, an application of the SQS-based method in DFT calculations of the dependence of twin boundary energies on Al content in Ti-Al hcp alloys is demonstrated.

II. METHODOLOGY

In this section we describe details associated with the calculation of planar defect energies in alloys, employing supercell models in conjunction with the SQS approach for configurational averaging. The focus is on hcp alloys, considering three types of planar defects that are relevant to their mechanical properties: twin boundaries, unstable stacking faults and free surfaces. Specifically, we consider the $\{11\bar{2}1\}$ twin boundary, which is observed in the deformation microstructures of many hcp metals and alloys such as Ti, Re, Mg and Be[8,46–48]. Further we consider calculations of the generalized stacking fault (GSF) surface corresponding the common $\{1\bar{1}00\}$ $\langle11\bar{2}0\rangle$ slip system in hcp metals. Finally, the energies of $\{1\bar{1}00\}$ free surfaces are considered. We begin by describing the supercells and planar averaging employed for the modeling of these planar defects and the calculation of their energies. A discussion of the generation of the SQS models is then presented, followed by the computational details for the present studies.

A. Supercell Geometries

1. Twin Boundaries

The $\{11\bar{2}1\}$ twin boundary in the hcp structure can be described by 4 twinning elements $K_1 = (11\bar{2}1)$, $K_2 = (0001)$, $\eta_1 = [\bar{1}\bar{1}26]$ and $\eta_2 = [11\bar{2}0]$.[49,50] These twinning elements denote the twinning plane, conjugate twinning plane, twinning direction and conjugate twinning direction, respectively. The amount of twinning shear for this twin is $S = \gamma^{-1}$, where $\gamma = c/a$, i.e. the axial ratio of the c and a lattice parameters. Since hcp metals have 2 atoms in the motif corresponding to a hexagonal Bravais lattice-point, in general twins cannot be formed by the application of a homogeneous twinning shear alone, and additional atomic shuffles are required[49,51]. For the $\{11\bar{2}1\}$ twin boundary, the required atomic shuffles on both sides of the twin boundary plane are given by the vector $\tau = \pm0.5\,[1\bar{1}00]$[51].

In this work, the $\{11\bar{2}1\}$ twin boundary is constructed directly from an appropriate bulk cell as follows. First, as illustrated in Fig. 1 (a) the bulk cell is constructed with lattice vectors parallel to $\mathbf{a} = [10\bar{1}2]$, $\mathbf{b} = [10\bar{1}0]$ and $\mathbf{c} = [\bar{1}100]$. The dimension along $\mathbf{b}$ is 8 times the conventional bulk hcp lattice constant a. This dimension is chosen such that the bulk cell can be employed to build twin boundary geometries, with sufficient spacing between the twin and its periodic images to minimize spurious interactions. The required bulk cell size is established by convergence studies, which show for the systems considered in this work that beyond 6 planes from the twin boundary, the solute formation energies are essentially converged to the bulk value. This leads to a bulk cell consisting of 64 atoms. The distance separating the two twins in the periodic cell that is required to achieve converged interfacial energies is expected to be system dependent, such that the dimensions of the cells employed in this work may not transfer directly to other alloy compositions. For each system, convergence testing

should be undertaken.

In the second step, the twin boundary cell is formed by i) applying a twinning shear S to all atoms located on one side of the twin plane in the middle of the supercell (i.e., half way along the periodic length along the **b** direction), followed by ii) an atomic shuffle on one side of the twin plane, as described above. This results in a twinned cell with a twin plane in the middle and another on the edge of the cell, as illustrated in Fig. 1 (b). Note that there exists a direct mapping between atoms in the bulk and twinned cell, which is important for the application of the SQS approach. Further note that several possible independent locations exist in the bulk cell where the twin plane can be inserted. In Fig. 1, the twin is placed in the center of the cell, but this location is arbitrary and for studying planar defects in alloys, we have found improved accuracy when results are averaged over all possible locations of the planar interface, as described below.

For calculations of the twin boundary energy, the initial and final geometries shown schematically in Figs. 1 (a) and (b), respectively, are calculated and γ_t is extracted from the energy difference divided by the twin boundary surface area, taking into account the presence of two twin boundaries per periodic supercell. In the energy calculations for the twinned supercells ionic relaxations are performed, and the dimension perpendicular to the twin plane is relaxed, while holding the periodic distances in the twin plane (i.e., along **a** and **c**) fixed at the values dictated by the bulk hcp supercell.
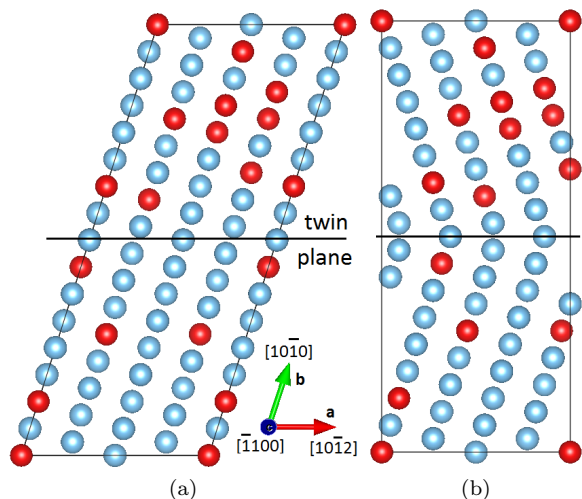

FIG. 1: Example supercell geometry for (a) a bulk alloy with an appropriate orientation for defect calculations and (b) a $\{11\bar{2}1\}$ twin boundary cell, formed from the bulk after an appropriate combination of shear and shuffle. This figure shows a projection along the $[\bar{1}100]$-direction. The twin-plane is inserted in the center of the bulk cell and is also indicated.

2. Unstable Stacking Faults and Surfaces

Supercells for the calculation of the $\{1\bar{1}00\}\langle11\bar{2}0\rangle$ GSF energy, and the $\{1\bar{1}00\}$ surface energy are constructed by choosing lattice vectors in the directions $\mathbf{a} = [11\bar{2}0]$, $\mathbf{b} = [0001]$ and $\mathbf{c} = [1\bar{1}00]$, as illustrated in Fig. 2 (a). As above, the cells contain atomic configurations derived from the SQS algorithm described in the next section. When performing calculations of the GSF and surface energies, two planes are picked which will be (i) rigidly shifted along the $\mathbf{a} = [11\bar{2}0]$ direction in order to create a stacking fault, or (ii) separated by a vacuum layer in order to create two free surfaces. All possible choices for these neighboring planes are considered and the planar energies are derived by averaging results over these different sets of planes.

Considering first the calculation of the GSF energy, the bulk supercell is set up initially to be periodic along all three directions. The size of the original bulk supercell is three times the bulk hcp lattice constant (a) along **a**, two times the bulk hcp lattice parameter (c) along **b**, and there are 6 layers of prismatic planes (for each plane there are two sub-layers) along **c**, resulting in a total number of 72 atoms. To calculate the GSF energy and γ_{USF} in particular, all atoms in the half supercell below a given $(1\bar{1}00)$ plane in the middle of the supercell are rigidly shifted along the $[11\bar{2}0]$ direction with the slip distances set as 0, 0.35, 0.45, 0.5 and 0.6 a, respectively. These shifts are accommodated by distorting the unit cell to have an angle different from 90 degrees between the **a** and **c** directions, so there is only one stack fault interface in this periodic supercell, as illustrated in Fig. 2 (b). For each slip vector, all the atoms in the supercells are relaxed along the **c** direction but fixed along the **a** and **b** directions. The supercell size along the $\mathbf{c} = [1\bar{1}00]$ direction is also relaxed to remove the normal stress perpendicular to the $(1\bar{1}00)$ plane. The GSF energy surface is plotted based on the energy increase at these slip distances relative to the undeformed structure, and γ_{USF} is derived by interpolating the maximum point on the GSF curve.

To compute the $\{1\bar{1}00\}$ surface energy γ_{s}, we start by calculating the energy of the bulk supercell illustrated in Fig. 2 (a). This reference energy is computed with periodic boundaries in all three directions, the same as the reference supercells for GSF calculations. The energy of this periodic bulk supercell reference energy is then compared to the energy obtained for the supercell illustrated in Fig. 2 (c), where a vacuum layer of 15 Å is introduced in the middle of the relaxed supercell, giving rise to two $\{1\bar{1}00\}$ surface planes. From the energy difference of these two supercells, divided by twice the cross-sectional area parallel to the surface planes, the value of γ_{s} is derived. In the calculations of the energies of the bulk and surface supercells the positions of all atoms are relaxed.
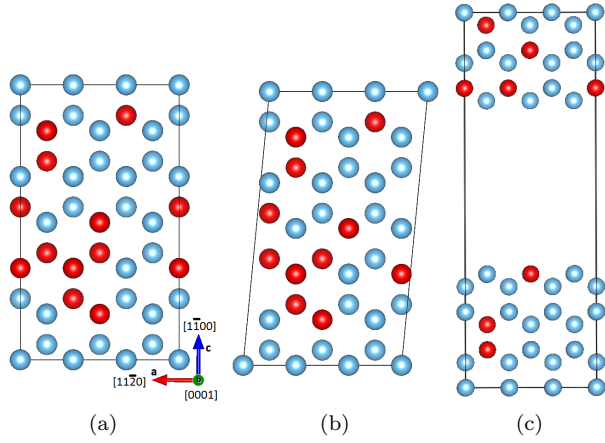
FIG. 2: Supercell geometry for (a) a bulk cell with an appropriate orientation for defect calculations (b) calculation of the generalized stacking-fault energy and (c) calculation of free-surface energies. These figures show a projection along the [0001]-direction.

B. SQS Generation

The SQS structures were developed for each of the bulk supercells defined in the previous subsection at different compositions starting at approximately 3 at.% solute, up to a maximum concentration of 25 at.% solute, with increments of approximately 3 at.%. A genetic algorithm (GA) was used for optimizing the SQS configuration, as described below. GA's have been employed in the materials-science community in the study of different topics such as crystal-structure prediction[52–54] and in the construction of cluster expansions[55,56].

We illustrate the use of a GA for the optimization of SQS with an example. Consider a hypothetical A-B binary alloy consisting of 16 atoms, at composition $A_{12}B_4$. The occupations of A and B atoms across the atomic sites are encoded as a binary string, for example as follows: [0010100000100001]. Each entry in the string corresponds to a given atomic site and can be occupied by either an A-atom (represented by 0's) or a B-atom (represented by 1's). The ordering of the different atomic sites in the string is irrelevant, as long as it is consistent throughout the optimization process. The example alloy has B-atoms located at atomic sites with indices 3, 5, 11 and 16 and A-atoms otherwise.

The mating process entails combining pairs of parents (alloys) into offspring by means of a process called crossover[57,58]. This process can be illustrated as follows. Consider again the alloy configuration introduced above (referred to as P_1) but now also another alloy configuration referred to as P_2, given by the binary string [1000010000000011]. Crossover is performed by picking a random number N between 1 and 15, splitting the binary strings of the parents at this number and cross-combining them into two children. For example, con-

sider the case $N = 9$. We obtain 4 strings after splitting the parents, S_1, S_2, S_3, S_4:

$$\left[\underbrace{001010000}_{S_1} \underbrace{0100001}_{S_2} \right]$$

and $\left[\underbrace{100001000}_{S_3} \underbrace{0000011}_{S_4} \right]$. The crossover process combines these parents P_1 and P_2 into two children, P_3 and P_4. Child P_3 consists of S_1 and S_4: [0010100000000011] and P_4 consists of S_2 and S_3: [1000010000100001]. In order to perform this process at constant composition, a special type of crossover has to be used that preserves the number of 0's and 1's in the binary string. This type of crossover, called edge crossover[59], is used in this work, and is slightly more complex than the example described above.

Mutation refers to introducing "defects" in the mating process and is designed to escape from local minima that may occur during the optimization process (similar to the ability of simulated-annealing optimization to allow for energetically unfavorable moves). For the optimization of SQS, mutation is implemented by allowing for a small probability to swap a 0 and a 1 in each child in each iteration.

The optimization procedure is initiated by generating an initial population of 800 randomly generated configurations at a given composition. The selection method used is roulette wheel selection, in which selection probability for mating is proportional to the fitness score. Further, a 0.5 % probability of mutation is allowed and the algorithm is run for 1000 generations. In every iteration, the pairs of "fittest" (most random) alloys are allowed to produce offspring via crossover, while allowing for the possibility of mutation to take place. In practice, we found that after only about 100 generations the resulting optimum SQS had converged to the optimum near-random atomic correlation functions.

The objective function to be minimized for SQS optimization is the Euclidean difference norm between the vector describing the atomic correlation functions of a random solid solution, $\mathbf{x}^{random}$ and the vector describing the correlation functions of the finite-sized supercell $\mathbf{x}^{scell}$. The fitness of any given configuration is inversely proportional to this Euclidean difference norm $\left\| \mathbf{x}^{random} - \mathbf{x}^{scell} \right\|$. In this work, 6 atomic correlation functions are considered for pairs, and 3 for triplets. The 6 pair terms are obtained by selecting all pairs smaller than a distance r such that $r < 1.8a$, where a is the conventional lattice constant (nearest neighbor distance) for hcp in the basal plane. Further note that the relaxed hcp cell of Ti obeys $c \approx 1.585a$ (where c is the conventional lattice constant perpendicular to the basal plane), so that the nearest-neighbor atomic pairs perpendicular to the basal plane are included in the analysis. In addition, all triplets were selected that contain no pairs longer than a, leading to a total of 3 triplets. The point clusters are imposed by the desired composition for the SQS. The atomic correlation functions for both the random alloys

and the trial configurations are calculated using the alloy theoretic automated toolkit (ATAT)[60,61] and fed to the GA during the iterative optimization process. In defining the fitness function, we explored different weighing factors for the different pair and triplet clusters, e.g., giving higher weight in the difference norm to shorter pairs and/or to clusters with higher multiplicities. Several different sets of weights were explored and even though different SQS were obtained for each, we found minimal influence on the resulting planar defect energies.

For an optimized bulk SQS such as shown in Fig. 3, there are several choices for where the planar faults can be inserted. As an explicit example, Fig. 3 shows 8 possible locations for a twin-boundary plane within a 64-atom SQS. A single SQS cell contains (after the deformation process illustrated in Fig. 1 (a) and (b)) both a twin boundary at the center (location 5 in Fig. 3) as well as another at the periodic boundary at location 1. Hence, all possible twin planes can be considered with a single bulk SQS configuration that is deformed according to 4 separate shear modes. The local atomic environment and solute-concentration vary along the b-direction and hence, the twin-boundary energy will vary depending on the location of the twin plane in the supercell. As discussed above, planar defect energies are calculated by inserting the planar defect into different locations in a single SQS and taking an average over those individual configurations. For the calculation of twin boundary energies, periodic boundary conditions are employed and hence, the 8 possible twin planes (Fig. 3) are covered with only 4 distinct cells. Consequently, we do not obtain twin boundary energies for each of the 8 twin planes individually, but rather the sum of pairs. For example, if the bulk cell in Fig. 3 is sheared into a twin cell (such as illustrated in Fig. 1), the sum of twin boundary energies at locations 5 and 1 is obtained. Other configurations are obtained by translating all atoms in the bulk cell in 3 by one unit along the b lattice vector. As such, all combinations of twin planes considered are 1 & 5, 2 & 6, 3 & 7 and 4 & 8, yielding a total of 4 calculations on twinned cells and a single calculation on the reference bulk cell. The averaging procedure simply entails taking the mean of all these computed planar defect energies. Similarly, for the GSF and surfaces, there are six independent choices for the location of the surfaces and planar defect energies are computed by averaging over each.

C. Computational Methods

1. Embedded-Atom-Method Calculations

The purpose of the computations based on classical embedded-atom-method (EAM) potentials performed in this work is to enable a comparison of planar defect energies obtained from the relatively small SQS supercells, with benchmark results obtained by direct configurational averaging over much larger supercells having
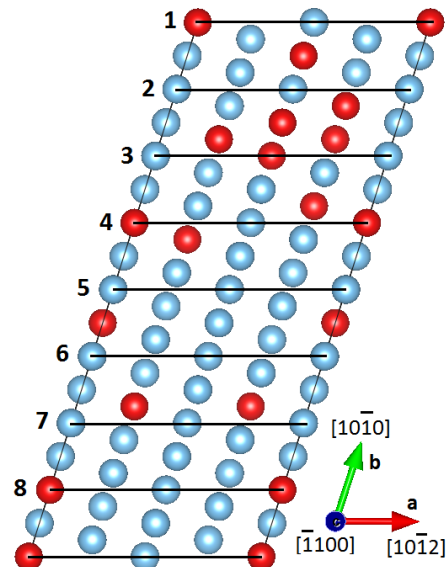

FIG. 3: Illustration of an SQS and configurational averaging-procedure used to compute the $\{11\bar{2}1\}$ TB energy. For the TB-calculations, a configurational average over 8 configurations within a single SQS-cell is employed. This figure shows a projection along the $[1\bar{1}00]$-direction.

a size that ensures minimal effects of periodic boundary conditions and accurate configurational averaging. These large cells are beyond the size that can be modeled directly by DFT, but their energies can be readily calculated using EAM potentials. Specifically, due to the small computational cost of performing EAM energy calculations, we consider as our benchmark results obtained from supercell models containing up to a million (1M) atoms in total, with the configuration of A and B atoms generated randomly for a given fixed overall alloy composition. These very large 1M cells are assumed to provide adequate configurational averaging to yield converged planar-defect energies for random solid solutions. As in the small SQS models, the planar defect energy is computed by subtracting the energy of the bulk cell from the energy of the corresponding cell containing the desired twin, surface or unstable stacking-fault defect. We note that, due to the large size of the 1M atom supercells, planar averaging, as is done for the smaller SQS cells, was not required and all benchmark values are derived by considering a single location for the interface in the supercell. This procedure can be repeated for different solute compositions such that the concentration dependence of the defect energies for a random substitutional alloy can be computed. The results computed as such from the 1M cells form a benchmark for the defect energies in disordered substitutional alloys, and the aim is to assess the accuracy of the SQS models in reproducing these values. In all of the EAM calculations we consider the defect energies for hcp-based Ti-Al alloys, modeled with the potential of Zope and Mishin[45].

2. Density Functional Theory Calculations

In addition to the EAM modeling described in the previous section, we also demonstrate the application of the SQS methodology in DFT-based computations of the concentration dependence of $\{11\bar{2}1\}$ twin boundaries in hcp-based Ti-Al alloys. These DFT calculations were performed using the Vienna Ab Initio Simulation Package (VASP)[62,63]. The VASP calculations made use of the generalized-gradient-approximation exchange-correlation energy due to Perdew-Burke-Ernzerhof generalized gradient functional (PBE-GGA)[64]. All calculations made use of the projector augmented wave (PAW) formalism[65,66], in which the potentials for Ti (Al) treat $4s$ and $3d$-states ($3s$ and $3p$ states) as valence. An energy cutoff for the plane waves of 600 eV was used, and smearing of the electronic occupancies was performed using the Methfessel-Paxton scheme[67], with a broadening of 0.05 eV. Integrations in the Brillouin zone were carried out using Monkhorst-Pack k-point sampling[68] with a density chosen such that the number of k-points in the first Brillouin zone times the number of atoms in the cell equals approximately 25,000.

III. RESULTS AND DISCUSSION

A. Embedded Atom Method Results

1. Twin Boundary Energies

In Fig. 4, the variation of the $\{11\bar{2}1\}$ twin boundary energy is plotted as a function of the atomic concentration of Al. The (red) open circle symbols are the benchmark results, labeled "Random-1M," obtained from a supercell containing approximately a million atoms, with randomly generated atomic configurations. The results labeled "SQS-64" were obtained by averaging over the different possible positions of the twin planes in SQS 64-atom supercells, generated as described in the previous section, and are plotted with (blue) filled squares. The error bars for the SQS results denote one standard deviation in the values obtained for the different choices of the TB plane position, and provide a measure of the width of the distribution in the individual planar defect energies. In addition, the individual SQS planar fault energies, corresponding to the different choices for the twin-boundary plane, are shown in Fig. 4 and labeled "SQS raw data".

It can be seen from Fig. 4 that the SQS and benchmark results at each composition agree to within approximately 10 %. To further quantify the degree of agreement between the SQS and benchmark results, we consider the composition dependence of the twin-boundary energies, as characterized by a dimensionless parameter, defined as $\eta_\gamma = (\partial\gamma/\partial x)/\gamma_0$, where γ represents the planar defect energy corresponding to the atomic fraction of Al in
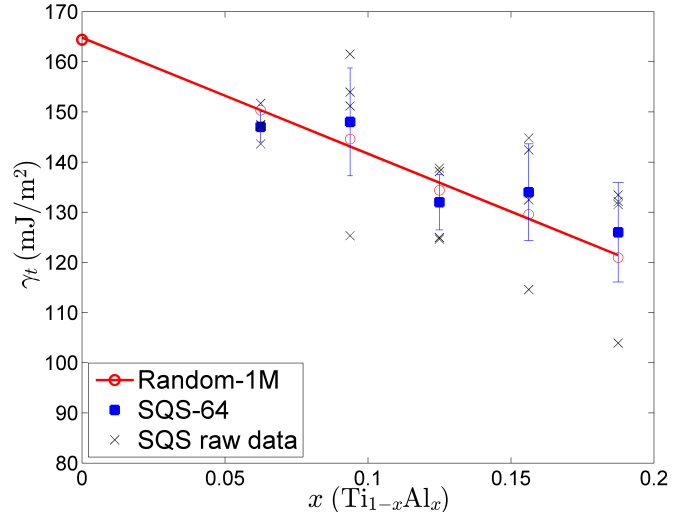

FIG. 4: $\{11\bar{2}1\}$ twin boundary energies (γ_t) in $\mathrm{Ti}_{1-x}\mathrm{Al}_x$ alloys calculated using EAM potentials with two different supercell models: the benchmark Random-1M supercell, and the SQS-64 supercell. For the 64-atom SQS supercell, the results are an average over 8 planes in one SQS, and the error bars are standard deviations. The "SQS raw" data points at each composition correspond to the individual values of the planar fault energies for different positions of the twin boundary. The line through the benchmark Random-1M results is a guide to the eye.

the $\mathrm{Ti}_{1-x}\mathrm{Al}_x$ binary alloy, and γ_0 is the defect energy for the pure-Ti reference state. The results obtained for η_γ, from a linear least squares fit (forced through the pure-Ti value) to the data sets in Fig. 4 are listed in Table I. The SQS-64 supercells yield a value for η_γ that is about 10 % larger in magnitude than the corresponding value for the random-1M cells. Overall, the results in this section suggest that for atomic fractions of solute up to approximately $x = 0.25$, estimates of the twin boundary energy at each composition converged to within about 10 % (10 mJ/m^2) can be derived by averaging results for 8 planes of a single 64-atom SQS-supercell configuration.

It can be seen from Fig. 4 that the raw twin boundary energies for each composition broadly follow the overall downward trend with increasing solute concentration. However there are several outliers, in particular near 9 at. % solute, which underscores the importance of the averaging procedure proposed in this work in order to obtain reliable statistics for the random alloy. For the $\{11\bar{2}1\}$ twin boundary, convergence testing of the composition dependence of the fault energy is performed with respect to the size of the SQS. By consecutively doubling both dimensions of the cell in the twin plane (with respect to the 64-atom cell), we obtain cells consisting of 256, 576 and 1024 atoms, respectively. Table I shows the composition dependence of the twin energy obtained with the 64-

SQS, 256-SQS, 576-SQS and 1024-SQS supercells. Based on the results in Table I, the SQS-64 and SQS-256 both yield results within 10 % of the benchmark Random-1M values. Further, it can be seen that increasing the size of the SQS leads to gradual convergence of the results towards the benchmark Random-1M values. In particular, values obtained with the 576-atom and 1024-atom SQS yield comparable agreement (within approximately 1 %).

It is noted that atomic relaxations have profound effect on the calculated $\{11\bar{2}1\}$ twin-boundary energy. The as-constructed $\{11\bar{2}1\}$ twin boundary has several pairs of atoms bond lengths contracted by approximately 25 %, relatively to bulk hcp. This is heavily penalized by the repulsive energy term in the interatomic potentials, and leads to high unrelaxed planar fault energies. Allowing for atomic relaxations drives down the planar fault energy to lower values: in the case of elemental Ti from 650 mJ/m^2 (unrelaxed) to 164 mJ/m^2 (relaxed), amounting to a reduction of 75 %. For the SQS Ti-Al alloys, similar or slightly larger effects caused by the atomic relaxations are observed, ranging from approximately 80 to 90 %, depending on the precise composition and SQS configuration. We believe this slightly larger effect of relaxations in the alloys can be attributed to atomic size mismatch: Al-atoms are smaller than Ti-atoms and hence, the Ti-atoms are less constrained and can more freely relax into their lower energy configurations in the alloy.

2. Unstable Stacking-Fault Energies

In Fig. 5 the unstable stacking-fault energy γ_{USF} results are plotted as a function of solute concentration, based on calculations employing the 72-atom SQS supercells illustrated in Fig. 2 (a)-(b), and benchmark Random-1M supercells. As in the previous section, the error bars on the SQS results were obtained from the standard deviation in the six values corresponding to different choices for the prismatic plane defects. In addition, the individual SQS USF energies, corresponding to the different choices for the stacking-fault plane, are shown in Fig. 5 and labeled "SQS raw data".

A roughly linear variation of γ_{USF} with Al concentration is obtained for the benchmark Random-1M supercells, up to the concentration of $x = 0.25$ considered in the calculations. Compared to these benchmark values, those obtained with the smaller 72-atom SQS supercell show significantly more scatter. However, for all compositions the SQS-72 supercells produce values for γ_{USF} that agree to within approximately 10 mJ/m^2 (≈ 2.5 %) with the benchmark values. The concentration dependence of γ_{USF} is slightly underestimated relative to the benchmark results, by 5.3 %, with the SQS-72 supercells, as shown in Table I. Further, the raw SQS results obey the upward trend in the defect unstable stacking fault energy, although several data points show large deviations from the average value, by up to approximately 50 mJ/m^2. The averaging procedure mitigates this effect
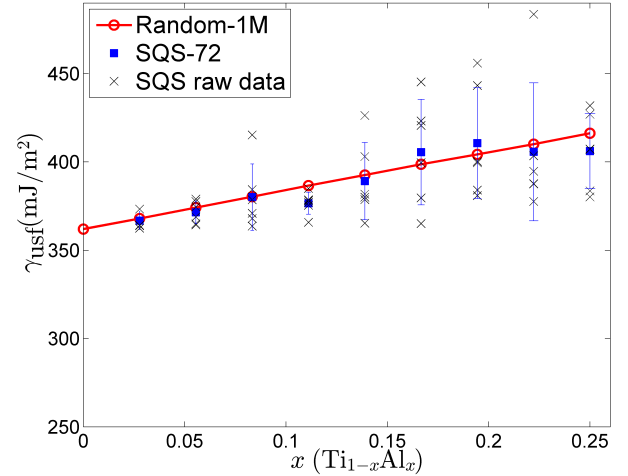

FIG. 5: Unstable stacking fault energies in $Ti_{1-x}Al_x$ alloys calculated using EAM potentials with two different supercell models: the benchmark Random-1M supercell, and the SQS-72 supercell. For the 72-atom SQS supercell, the results are an average over 6 planes in one SQS, and the error bars are standard deviations. The "SQS raw" data points at each composition correspond to the individual values of the unstable stacking fault energies for different positions of the stacking-fault plane. The line through the benchmark Random-1M results is a guide to the eye.

and leads to a value of the USF energy that shows good agreement with the benchmark results.

3. Surface Energies

In Fig. 6 results for the calculated $\{1\bar{1}00\}$ surface energy (γ_{s}) are plotted as a function of Al concentration. As in Fig. 5 results are plotted for the benchmark supercells, and for the 72-atom SQS supercells. The average values and error bars for the SQS cells have again been obtained from an average over 6 planes. The averaged values obtained from the SQS-72 supercells show agreement with the benchmark results to within 10 mJ/m^2, or less than 1 % of the magnitude of γ_{s}. As for the twin boundary and unstable stacking fault energies, the individual "SQS raw data" surface energies, corresponding to the different choices for the surface plane in the SQS structure, follow the overall composition trend, but averaging is required to obtain good agreement with the benchmark results.

To compare the predictions of the 72-atom supercells for the concentration dependence of γ_{s}, we fit each data set in Fig. 6 with a parabola, to account for the non-linear behavior that can clearly be observed in the figure. The composition dependence, as characterized by the η_γ parameter, is evaluated for two compositions and

TABLE I: Concentration dependence of planar defect energies in hcp $Ti_{1-x}Al_x$ solid solutions, $\eta_\gamma = (\partial\gamma/\partial x)/\gamma_0$, as calculated with EAM interatomic potentials, using benchmark Random-1M and SQS-72/64 supercell models. For the twin boundary, 64-atom SQS supercells are employed, and for the surface and stacking fault energies, 72-atom SQS supercells are employed. For comparison, the results for the twin boundary, using several larger SQS are also shown. The Al atomic fraction is denoted by x for the $\{1\bar{1}00\}$ surface.

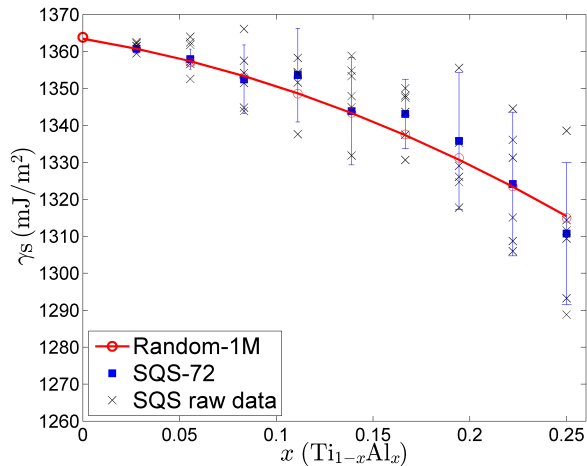| Planar defect		EAM (Random-1M)	EAM (SQS)
$\{11\bar{2}1\}$ Twin (64-atom SQS)		-1.56	-1.43
$\{11\bar{2}1\}$ Twin (256-atom SQS)		-1.56	-1.47
$\{11\bar{2}1\}$ Twin (576-atom SQS)		-1.56	-1.58
$\{11\bar{2}1\}$ Twin (1024-atom SQS)		-1.56	-1.57
$\{1\bar{1}00\} \langle 11\bar{2}0\rangle$ USF		0.57	0.55
$\{1\bar{1}00\}$ Surface	$x \approx 0.08$	-0.12	-0.10
$\{1\bar{1}00\}$ Surface	$x \approx 0.195$	-0.19	-0.22

FIG. 6: $\{1\bar{1}00\}$ surface energies in $Ti_{1-x}Al_x$ alloys calculated using EAM potentials with two different supercell models: the benchmark Random-1M supercell, and the SQS-72 supercell. For the 72-atom SQS supercell, the results are an average over 6 planes in one SQS, and the error bars are standard deviations. The "SQS raw" data points at each composition correspond to the individual values of the surface energies for different positions of the surface plane. The line through the benchmark Random-1M results is a guide to the eye.

the Random-1M and SQS-72 values are compared in Table I. The agreement is seen to be at the level of 15-17 % at the two different compositions listed.

4. SQS Versus Random Supercells

It is interesting to consider whether the SQS configurations used in the comparisons above lead to improved agreement with benchmark results, relative to values derived from supercells with the same size, but with the atomic configurations generated randomly rather than by the SQS algorithm. In other words, it is of interest to consider whether the extra work that is required to generate the SQS configurations for a given defect supercell leads to a significant increase in accuracy. To test this, we have undertaken a statistical analysis comparing the performance of random and SQS supercell configurations against the benchmark values. Results of such tests are reported in this section for the specific case of the twin-boundary planar defects, but similar conclusions were reached for the GSF and surface defects.

We begin by generating a large number of randomly occupied structures and rank these according to a performance metric that measures how close the pair and triplet correlation functions are to the values for a random alloy with the same composition. For the dilute compositions, an exhaustive enumeration[69–71] is performed of *all* symmetrically inequivalent atomic configurations at a fixed composition. For the more concentrated alloys, exhaustive enumeration is beyond reach and we instead generate a million symmetry inequivalent structures. These configurations are then ranked from #1, indicating the best agreement with random correlation functions, in ascending order towards the worst. For all the configurations generated, the $\{11\bar{2}1\}$ twin boundary energy is calculated by planar averaging and it is examined how well the resulting defect energies approximate the benchmark Random-1M results. In this section, Ti-Al alloys with a solute concentration of 12.5 at. % Al are considered, but similar conclusions hold for different compositions.

In total, a million symmetry-inequivalent alloys are generated at a composition of $Ti_{56}Al_8$ and for each, the atomic correlation functions (6 pairs, 3 triplets) are calculated. These are referred to as $corr^{SQS}$. The million structures are then ranked according to the metric $\|corr^{SQS} - corr^{Random}\|$. Smaller values for $\|corr^{SQS} - corr^{Random}\|$ indicate a configuration that is a better approximation of the true random alloy. Figure 7 shows the distribution of this metric over the million structures, together with a β-distribution that is fit through the data. The mean of the distribution is approximately 0.26, the best SQS structures exhibit qualities

$\|corr^{\text{SQS}} - corr^{\text{Random}}\| \approx 0.10$ and for the worst configurations $\|corr^{\text{SQS}} - corr^{\text{Random}}\| \approx 0.65$.
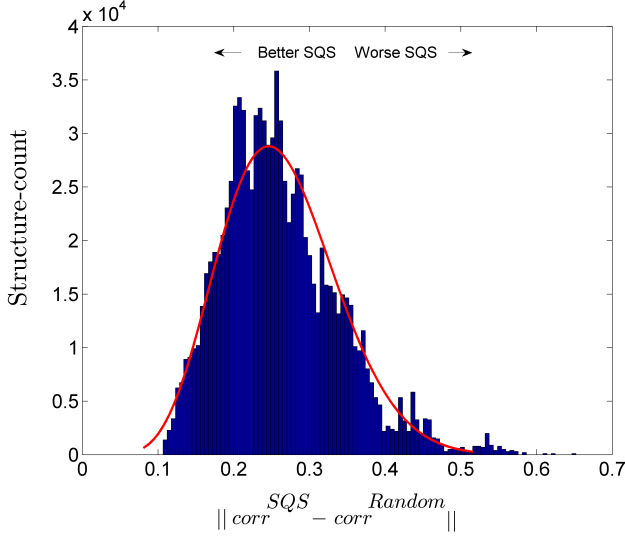

FIG. 7: The distribution of $\|corr^{\text{SQS}} - corr^{\text{Random}}\|$ over a million substitutional configurations for an hcp Ti$_{56}$Al$_8$ bulk alloy. A β-distribution is fit to the data and plotted by the solid (red) line in the histogram.

It is now addressed how well the structures used to generate Fig. 7 perform in their prediction of $\{11\bar{2}1\}$ twin boundary energies, compared with the Random-1M benchmark results. To this end, the million structures are split-up in 1,000 bins of 1,000 structures, where the first bin represents the 1,000 best configurations (corresponding to $\|corr^{\text{SQS}} - corr^{\text{Random}}\| \approx 0.10$), the second bin represents the second best group of configurations, and so forth. The last bin corresponds to $\|corr^{\text{SQS}} - corr^{\text{Random}}\| \approx 0.65$ and represents the bin containing the worst performing configurations. It is next examined for each of the bins how large the probability is that a structure picked at random from the bin yields a $\{11\bar{2}1\}$ twin boundary energy that is within 10 % of the Random-1M benchmark value. The results are shown in Fig. 8, in which a second order polynomial is fit through the calculated probability data. The horizontal axis again represents the value of $\|corr^{\text{SQS}} - corr^{\text{Random}}\|$, as in Fig. 7. The vertical axis in Fig. 8 represents $P\left(\|\left(\gamma_t^{\text{SQS}} - \gamma_t^{\text{Random}}\right)/\gamma_t^{\text{SQS}}\| < 0.1\right)$, i.e., the probability that a configuration in the bin and the random-1M benchmark twin-boundary energies are within 10 %.

Note that the above analysis was based on a total of 5 calculations for each 64-SQS at every composition and in total 2 calculations for each Random-1M cell at every composition. For the Random-1M cell, 1 calculation of the energy of the (atomically relaxed) bulk cell is required, together with 1 calculation of the energy of the (atomically relaxed) twinned cell. For the 64-SQS, 1 calculation of the (atomically relaxed) bulk cell is required, together with 4 calculations on the 64-SQS twin

cells. Owing to periodic boundary conditions, each calculation on a 64-SQS twin cell yields the average energy of 2 distinct twin boundaries, hence all 8 distinct planes are covered by these 4 calculations.
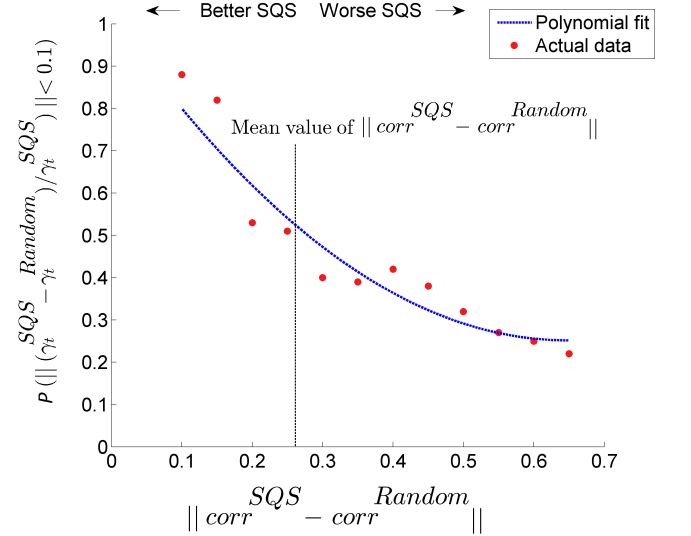

FIG. 8: Probability of reproducing the Random-1M twin energies to within 10 % as a function of the metric $\|corr^{\text{SQS}} - corr^{\text{Random}}\|$. The curve indicates a second order polynomial, fit to the calculated data.

Figure 8 shows clearly that among the best SQS structures (i.e., amongst the configurations with the lowest values of $\|corr^{\text{SQS}} - corr^{\text{Random}}\|$), there is a significantly higher probability of reproducing the Random-1M results for the $\{11\bar{2}1\}$ twin boundary energy than among the poorly performing configurations. For example, in the bin containing the best configurations, approximately 80 % of the structures reproduce the Random-1M twin energies to within 10 %. On the other hand, in the bin containing the configurations with the highest values of $\|corr^{\text{SQS}} - corr^{\text{Random}}\|$, only 25 % of the structures reproduce the Random-1M twin energies to within 10 %. Structures that are located near the mean of the distribution reproduce the Random-1M energies to within 10 % in approximately 50 % of the cases. Hence, we conclude that a high-quality SQS structure is expected statistically to perform significantly better than structures generated by random occupations.

B. Density Functional Theory Results

As an illustration of the use of the SQS approach in combination with DFT-based total-energy calculations, we plot in Fig. 9 calculated results for the $\{11\bar{2}1\}$ twin boundary as a function of Al concentration in Ti$_{1-x}$Al$_x$ hcp-based solid solutions. The DFT results were obtained with a 64-atom SQS supercell, averaging over the different choices for the TB plane position, as above. The

average values and standard deviations obtained by DFT are plotted with filled circles, and the results are compared to those obtained from the EAM employing the same SQS approach, which are reproduced in the lower panel.
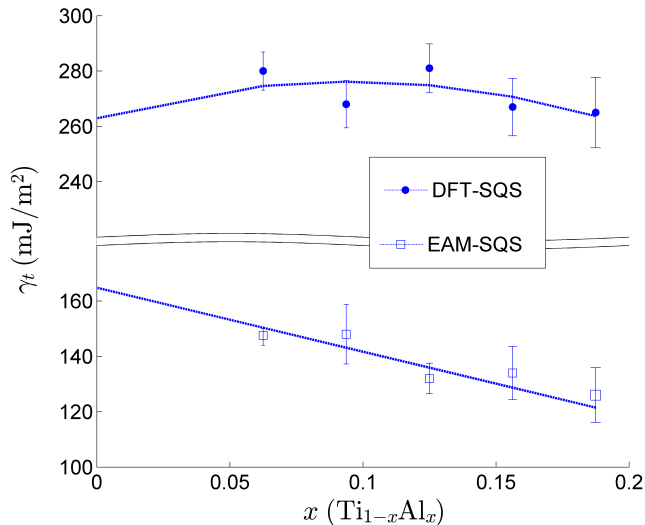

FIG. 9: $\{11\bar{2}1\}$ twin boundary energy γ_t in $Ti_{1-x}Al_x$ alloys calculated with 64-atom SQS supercells by DFT and EAM. The results plotted are averaged over 8 planes per supercell, with error bars denoting standard deviations. The lines are guides to the eye.

It is seen in Fig. 9 that the EAM underestimates the $\{11\bar{2}1\}$ twin boundary energy significantly with respect to the DFT value for pure Ti. We further note that EAM and DFT predict different trends of twin energy versus Al concentration. Whereas EAM predicts a monotonic and almost linear decrease of the $\{11\bar{2}1\}$ twin boundary energy with increasing Al content, the DFT calculations predict a much weaker concentration dependence.

It should be emphasized that the differences between EAM and DFT observed here are not a result of the SQS planar averaging, but a reflection of inaccuracies in the classical potential model for twin boundary energies in Ti-Al alloys. This is apparent based on the discrepancies for the results for pure Ti. Additionally, we have used the 64-atom supercell models with one Al solute atom present to compute segregation energies to the $\{11\bar{2}1\}$ twin boundary. It is found that the EAM potential predicts an energetic preference of an individual Al-atom to segregate to the twin plane and nearby planes, whereas DFT shows the opposite: the Al-atom prefers to reside in positions away from the twin. Since

DFT and EAM yield contradictory results even in this dilute limit, the discrepancies in the results obtained for more concentrated alloys are not surprising. We note that discrepancies between EAM and DFT are not uncommon in cases such as these where the property of interest (namely twin boundary energetics) were not included in the fitting of the EAM potential (e.g.,[72]). We note that it has also been shown that this EAM potential for Ti-Al alloys was not found to yield good agreement with DFT calculations for the concentration dependence of the elastic constants[73–75].

IV.   SUMMARY AND CONCLUSIONS

In the present work we have presented a method for computing the energetics of planar defects in random substitutional alloys employing an approach based on the use of the SQS formalism. It is shown using an EAM model for hcp-based Ti-Al alloys that averaging over results obtained for different planes in an SQS cell gives values for twin boundary, unstable stacking fault and surface energies that agree to within approximately 10 % with benchmark values obtained from direct configurational averaging using large supercells. The SQS-based supercells considered in this work are small enough such that their energies can be computed by DFT. This is demonstrated in DFT-based studies of the concentration dependence of $\{11\bar{2}1\}$ twin-boundary energies in hcp-based Ti-Al alloys. We anticipate that the method presented in this work will be useful in future DFT-based efforts aimed at alloy design. By combining results obtained with this approach within continuum theories of mechanical behavior, the SQS-approach described here provides a framework for investigating the effects of specific solute additions on the slip and twinning properties of alloys for targeted applications.

* Electronic address: maartendft@gmail.com
[1] J. R. Rice and R. Thomson, Philosophical Magazine **29**, 73 (1974).

[2] R. Thomson, Physical Review B **52**, 7124 (1995).
[3] R. Thomson and A. Carlsson, Philosophical Magazine A **70**, 893 (1994).

[4] S. Zhou, A. Carlsson, and R. Thomson, Physical review letters **72**, 852 (1994).

[5] J. R. Rice, Journal of the Mechanics and Physics of Solids **40**, 239 (1992), ISSN 0022-5096.

[6] M. J. Mehl, D. A. Papaconstantopoulos, N. Kioussis, and M. Herbranson, Physical Review B **61**, 4894 (2000).

[7] D. J. Siegel, Applied Physics Letters **87**, 121901 (2005).

[8] M. Yoo, Metallurgical Transactions A **12**, 409 (1981).

[9] N. Bernstein and E. Tadmor, Physical Review B **69**, 094116 (2004).

[10] D. J. Siegel, in *APS Meeting Abstracts* (2005), vol. 1, p. 26002.

[11] S. Ogata, J. Li, and S. Yip, Physical Review B **71**, 224102 (2005).

[12] S. Kibey, J. Liu, D. Johnson, and H. Sehitoglu, Acta Materialia **55**, 6843 (2007).

[13] P. Denteneer and W. van Haeringen, Journal of Physics C: Solid State Physics **20**, L883 (1987).

[14] S. Sandlöbes, M. Friák, S. Zaefferer, A. Dick, S. Yi, D. Letzig, Z. Pei, L.-F. Zhu, J. Neugebauer, and D. Raabe, Acta Materialia **60**, 3011 (2012).

[15] Z. Pei, M. Friák, S. Sandlöbes, R. Nazarov, B. Svendsen, D. Raabe, and J. Neugebauer, New Journal of Physics **17**, 093009 (2015).

[16] J. Hartford, B. Von Sydow, G. Wahnström, and B. Lundqvist, Physical Review B **58**, 2487 (1998).

[17] B. Paul Burton, A. van de Walle, and H. T. Stokes, Journal of the Physical Society of Japan **81**, 014004 (2011).

[18] Y. Li and P. A. Korzhavyi, Journal of Nuclear Materials **462**, 160 (2015).

[19] K. Limmer, J. Medvedeva, D. Van Aken, and N. Medvedeva, Computational Materials Science **99**, 253 (2015).

[20] M. Rahaman, V. Razumovskiy, B. Johansson, and A. Ruban, Philosophical Magazine **93**, 3423 (2013).

[21] M. Chandran and S. Sondhi, Journal of Applied Physics **109**, 103525 (2011).

[22] A. Abbasi, A. Dick, T. Hickel, and J. Neugebauer, Acta Materialia **59**, 3041 (2011).

[23] A. Reyes-Huamantinco, P. Puschnig, C. Ambrosch-Draxl, O. E. Peil, and A. V. Ruban, Physical Review B **86**, 060201 (2012).

[24] S. Sandlöbes, Z. Pei, M. Friák, L.-F. Zhu, F. Wang, S. Zaefferer, D. Raabe, and J. Neugebauer, Acta Materialia **70**, 92 (2014).

[25] L. Vitos, J.-O. Nilsson, and B. Johansson, Acta Materialia **54**, 3821 (2006).

[26] S. Lu, Q.-M. Hu, B. Johansson, and L. Vitos, Acta Materialia **59**, 5728 (2011).

[27] A. Zunger, S.-H. Wei, L. G. Ferreira, and J. E. Bernard, Phys. Rev. Lett. **65**, 353 (1990).

[28] S.-H. Wei, L. G. Ferreira, J. E. Bernard, and A. Zunger, Phys. Rev. B **42**, 9622 (1990).

[29] A. Van de Walle, P. Tiwary, M. De Jong, D. Olmsted, M. Asta, A. Dick, D. Shin, Y. Wang, L.-Q. Chen, and Z.-K. Liu, Calphad **42**, 13 (2013).

[30] A. Dick, T. Hickel, and J. Neugebauer, steel research international **80**, 603 (2009).

[31] O. Güvenç, F. Roters, T. Hickel, and M. Bambach, JOM **67**, 120 (2015).

[32] H. Ebert, D. Koedderitzsch, and J. Minar, Reports on Progress in Physics **74**, 096501 (2011).

[33] W. Kohn and N. Rostoker, Physical Review **94**, 1111 (1954).

[34] J. Korringa, Physica **13**, 392 (1947).

[35] S. Crampin, D. Vvedensky, and R. Monnier, Philosophical Magazine A **67**, 1447 (1993).

[36] K. Wildberger, R. Zeller, and P. Dederichs, Physical Review B **55**, 10074 (1997).

[37] K. Wood and J. Pendry, Physical Review Letters **31**, 1400 (1973).

[38] J. MacLaren, S. Crampin, D. Vvedensky, and J. Pendry, Physical Review B **40**, 12164 (1989).

[39] F.-Y. Tian, N.-X. Chen, L. Delczeg, and L. Vitos, Computational materials science **63**, 20 (2012).

[40] T. Schulthess, P. Turchi, A. Gonis, and T.-G. Nieh, Acta materialia **46**, 2215 (1998).

[41] I. Abrikosov and H. L. Skriver, Physical Review B **47**, 16532 (1993).

[42] W. Li, S. Lu, Q.-M. Hu, S. K. Kwon, B. Johansson, and L. Vitos, Journal of Physics: Condensed Matter **26**, 265005 (2014).

[43] S. Huang, W. Li, S. Lu, F. Tian, J. Shen, E. Holmström, and L. Vitos, Scripta Materialia **108**, 44 (2015).

[44] M. de Jong, J. Kacher, M. H. F. Sluiter, L. Qi, D. L. Olmsted, A. van de Walle, J. W. Morris, A. M. Minor, and M. Asta, Phys. Rev. Lett. **115**, 065501 (2015).

[45] R. R. Zope and Y. Mishin, Physical Review B **68**, 024102 (2003).

[46] D. Bacon and V. Vitek, Metallurgical and Materials Transactions A **33**, 721 (2002).

[47] J. Morris, J. Scharff, K. Ho, D. Turner, Y. Ye, and M. Yoo, Philosophical Magazine A **76**, 1065 (1997).

[48] M. Yoo, J. Morris, K. Ho, and S. Agnew, Metallurgical and Materials Transactions A **33**, 813 (2002).

[49] Y. Minonishi, S. Ishioka, M. Koiwa, and S. Mobozumi, physica status solidi (a) **71**, 253 (1982).

[50] A. Crocker, Philosophical Magazine **8**, 1077 (1963).

[51] J. W. Christian and S. Mahajan, Progress in Materials Science **39**, 1 (1995).

[52] A. O. Lyakhov, A. R. Oganov, H. T. Stokes, and Q. Zhu, Computer Physics Communications **184**, 1172 (2013).

[53] C. W. Glass, A. R. Oganov, and N. Hansen, Computer Physics Communications **175**, 713 (2006).

[54] A. R. Oganov and C. W. Glass, Journal of Physics: Condensed Matter **20**, 064210 (2008).

[55] G. L. Hart, V. Blum, M. J. Walorski, and A. Zunger, Nature materials **4**, 391 (2005).

[56] V. Blum, G. L. Hart, M. J. Walorski, and A. Zunger, Physical Review B **72**, 165113 (2005).

[57] W. Paszkowicz, Materials and Manufacturing Processes **24**, 174 (2009).

[58] W. Paszkowicz, Materials and Manufacturing Processes **28**, 708 (2013).

[59] L. D. Whitley, T. Starkweather, and D. Fuquay, in *ICGA* (1989), vol. 89, pp. 133–40.

[60] A. Van de Walle, M. Asta, and G. Ceder, Calphad **26**, 539 (2002).

[61] A. van de Walle, Calphad **33**, 266 (2009).

[62] G. Kresse and J. Furthmüller, Phys. Rev. B **54**, 11169 (1996).

[63] G. Kresse and J. Hafner, Phys. Rev. B **47**, 558 (1993).

[64] J. P. Perdew, K. Burke, and M. Ernzerhof, Phys. Rev. Lett. **77**, 3865 (1996).

[65] P. E. Blöchl, Phys. Rev. B **50**, 17953 (1994).

[66] G. Kresse and D. Joubert, Phys. Rev. B **59**, 1758 (1999).

[67] M. Methfessel and A. T. Paxton, Phys. Rev. B **40**, 3616 (1989).

[68] H. J. Monkhorst and J. D. Pack, Phys. Rev. B **13**, 5188 (1976).

[69] G. L. Hart and R. W. Forcade, Physical Review B **77**, 224115 (2008).

[70] G. L. Hart and R. W. Forcade, Physical Review B **80**, 014120 (2009).

[71] G. L. Hart, L. J. Nelson, and R. W. Forcade, Computational Materials Science **59**, 101 (2012).

[72] E. Metsanurk, A. Tamm, A. Caro, A. Aabloo, and M. Klintenberg, Scientific reports **4** (2014).

[73] J. von Pezold, A. Dick, M. Friák, and J. Neugebauer, Physical Review B **81**, 094203 (2010).

[74] M. de Jong, W. Chen, T. Angsten, A. Jain, R. Notestine, A. Gamst, M. Sluiter, C. K. Ande, S. van der Zwaag, J. J. Plata, et al., Scientific data **2** (2015).

[75] L.-Y. Tian, Q.-M. Hu, R. Yang, J. Zhao, B. Johansson, and L. Vitos, Journal of Physics: Condensed Matter **27**, 315702 (2015).